Journal of Alloys and Compounds 966 (2023) 171613

Contents lists available at ScienceDirect

Journal of Alloys and Compounds

journal homepage: www.elsevier.com/locate/jalcom

Application of Bayesian optimization to the synthesis process of $BaFe_2(As,P)_2$ polycrystalline bulk superconducting materials

Akimitsu Ishii [a], Shinjiro Kikuchi [b], Akinori Yamanaka [c], Akiyasu Yamamoto [d,*]

[a] International Center for Young Scientists, National Institute for Materials Science, 1-2-1, Tsukuba, Ibaraki 305-0047, Japan
[b] Department of Applied Physics, Graduate School of Engineering, Tokyo University of Agriculture and Technology, 2-24-16, Koganei, Tokyo 184-8588, Japan
[c] Division of Advanced Mechanical Systems Engineering, Institute of Engineering, Tokyo University of Agriculture and Technology, 2-24-16, Koganei, Tokyo 184-8588, Japan
[d] Division of Advanced Applied Physics, Institute of Engineering, Tokyo University of Agriculture and Technology, 2-24-16, Koganei, Tokyo 184-8588, Japan

ARTICLE INFO

Keywords:
Superconducting material
Bayesian optimization
Process informatics
Phase purity

ABSTRACT

This study is the first application of Bayesian optimization to the synthesis process of superconducting materials. As a model case, the phase purity of $BaFe_2(As,P)_2$ polycrystalline bulks, which affects their superconducting properties, was improved by optimizing only the heat-treatment temperature using Bayesian optimization. We determined the optimal temperature among 800 candidates in 13 experiments, and a phase purity of 91.3 % was achieved. Moreover, the phosphorus doping level of the best sample approached the optimal doping level owing to a reduction in the impurity phase. Visualization of the Bayesian optimization process showed that a well-balanced global search and local optimization allowed us to obtain a rough correlation between the superconducting properties and experimental conditions and finely optimal experimental conditions over a wide range. These results demonstrate that Bayesian optimization is promising for optimizing the synthesis process of superconducting materials.

1. Introduction

Several properties of superconducting materials, such as critical current density and critical field, depend on their composition and synthesis process. In particular, in the case of polycrystalline superconducting materials including iron-based superconductors, MgB_2, and metallic superconductors, processing conditions (e.g., the heat-treatment temperature, time, and ramp rate) as well as the chemical composition of the starting powder affect the microstructure. Therefore, optimization of the synthesis process is essential to achieving improved superconducting properties.

Conventionally, synthesis process optimization in materials science has been conducted based on the experience, knowledge, and intuition of a human expert or using non-adaptive methods such as a factorial design or a response surface approach. Process informatics (PI), which uses data science techniques/methods to optimize experimental processes, has recently been performed [1–8]. Bayesian optimization [9] has attracted significant attention as a powerful tool for PI because it can find global optima using only a mini-database generated from a few experiments. Lambard et al. [1] improved the coercivity of Nd-Fe-B permanent magnets using a Bayesian optimization-assisted PI framework. Osada et al. [2] optimized the epitaxial growth process of Si thin films through a few experiments using Bayesian optimization. Chang et al. [3] used Bayesian optimization to maximize the growth rate of carbon nanotubes. Wang et al. [4] reviewed examples of the applications of Bayesian optimization to the processing of chemical products and functional materials. In addition, because Bayesian optimization can eliminate human intervention, it is capable of providing an autonomous experimental framework in which the synthesis processes are automatically optimized using robots. Xie et al. [5] developed a robotic platform using Bayesian optimization to accelerate the synthesis process of metal-organic frameworks with high crystallinity. Deneault et al. [6] developed an autonomous system using Bayesian optimization that optimized multiple parameters used in 3D printing to satisfy the target features. Gongora et al. [7] reported that a combination of Bayesian optimization and automated experiments maximized the toughness of materials fabricated by additive manufacturing. Bayesian optimization has also been used to assist human experts in determining experimental conditions [8]. Furthermore, several user-friendly applications have been developed for Bayesian optimization [10,11], facilitating its use for

* Corresponding author.
E-mail address: akiyasu@cc.tuat.ac.jp (A. Yamamoto).

https://doi.org/10.1016/j.jallcom.2023.171613
Received 17 May 2023; Received in revised form 21 July 2023; Accepted 31 July 2023
Available online 1 August 2023

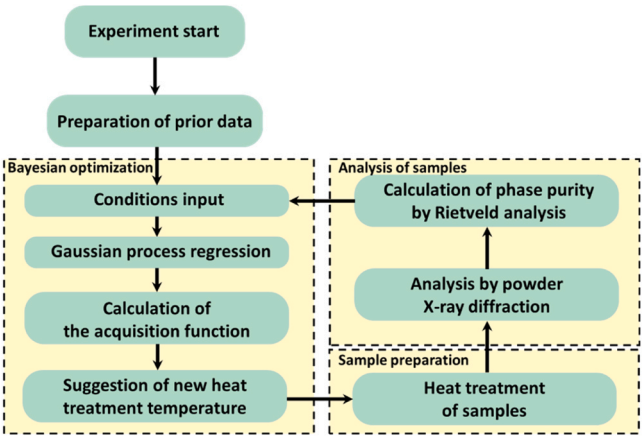

Fig. 1. Flowchart of process optimization for improving the phase purity of P-doped Ba122.

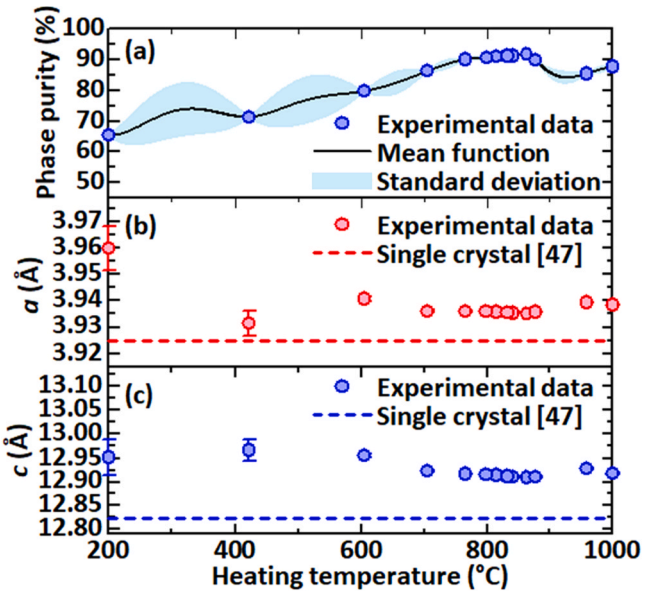

Fig. 2. Relationship between heating temperature and (a) phase purity, (b) lattice constant *a*, and (c) lattice constant *c*. Single crystal data from Ref. [47] are shown for comparison.

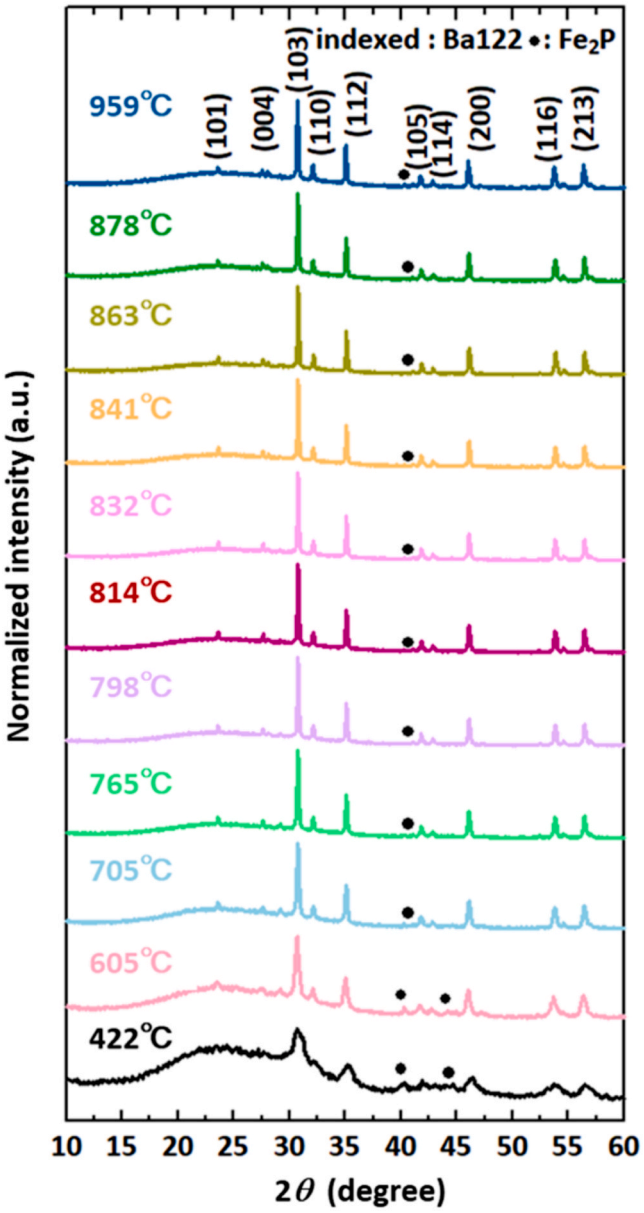

Fig. 3. Powder X-ray diffraction patterns of the samples with different heating temperatures.

the PI of various materials.

However, the optimization of the synthesis process for superconducting materials still strongly depends on the experiences of an expert owing to the lack of established mechanistic theories that link the process conditions to superconducting properties. Recently, Matera et al. [12] reported the maximization of the upper critical field of C-doped MgB_2 using the response surface method; however, no PI using Bayesian optimization was conducted for the synthesis process of superconducting materials. Therefore, this study is the first application of Bayesian optimization to the synthesis process of superconducting materials and focuses on the synthesis process of $BaFe_2As_2$ (Ba122) [13,14] polycrystalline bulk, which is one of the parent phases of iron-based superconductors (IBSC), as a model case.

IBSCs [15] are expected to have strong magnetic applications owing to their high critical temperature (T_c) and upper critical field (H_{c2}) [16] next to cuprate superconductors. Ba122 exhibits superconductivity by hole doping via potassium substitution at the barium site, electron doping via cobalt substitution at the iron site, and chemical pressure by phosphorus substitution at the arsenic site [17–19]. Ba122 shows a small electromagnetic anisotropy [20–25], an irreversible magnetic field close to H_{c2} [25], and a large critical grain boundary angle of 5–9°, approximately twice that of yttrium barium copper oxide [26,27]. These properties are relevant for the application of Ba122 materials in polycrystalline form.

An important aspect of the superconducting properties of Ba122 is the type of doping [28]. While focusing on T_c, studies found that 40 % K-doped Ba122 exhibits $T_c = 38$ K, 8 % Co-doped Ba122 exhibits $T_c = 23$ K, and 32 % P-doped Ba122 exhibits $T_c = 30$ K [17,19,29]. Among these doped Ba122 materials, P-doped Ba122 has the advantage of a high critical current density in thin films owing to the introduction of artificial vortex pinning centers [30–36]. Moreover, because of the uniqueness of superconductivity, manifested by isovalent doping, its physical properties have been extensively studied to elucidate its origin [37–39]. However, compared to other doped systems, establishing a material synthesis process for obtaining high-phase-purity samples is a challenge in P-doped systems. Phosphorus tends to form a stable compound with iron (Fe_2P), making it difficult to obtain single-phase P-doped Ba122 and also making it difficult to control the doping state of the

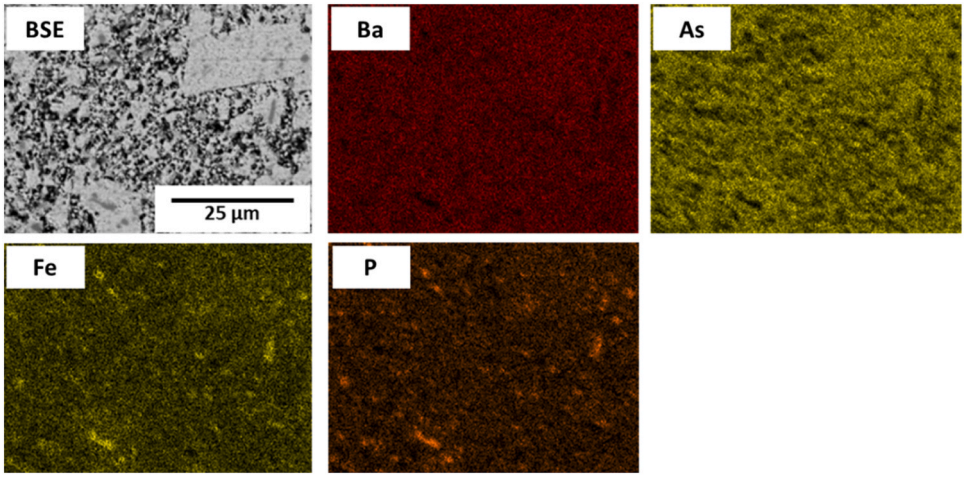

Fig. 4. Backscattered electron microscopy and elemental mapping images of Ba, As, Fe, and P for the polished cross-sectional surface of the sample heated at 863 °C.

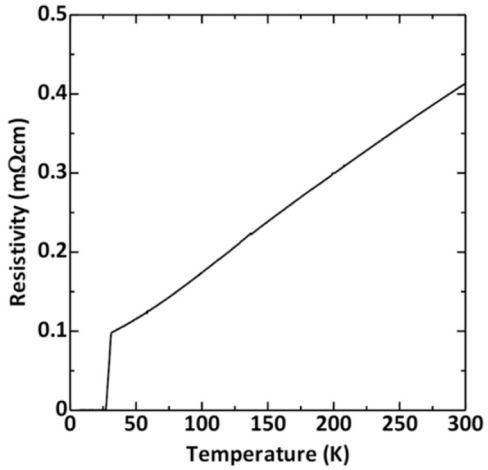

Fig. 5. Temperature dependence of resistivity for the $BaFe_2(As,P)_2$ bulk sample sintered at 863 °C.

superconducting phase because of the incorporation of phosphorus within the secondary phase [40,41]. According to Contarino et al. [40], the formation of impurity phases is caused by ion diffusion due to heat-treatment at high temperatures. Additionally, they state that suppressing the phosphorus-containing impurity phase is key to improving the superconducting properties of P-doped Ba122. Therefore, high superconducting properties are expected to be achieved by optimizing the heat-treatment conditions and maximizing the phase purity.

In this study, using Bayesian optimization, the phase purity of P-doped Ba122 polycrystalline bulks was improved by optimizing the heat-treatment process. Although the heat-treatment process of P-doped Ba122 has several design parameters such as temperature, time, and heating rate, this study optimized only the temperature, which is assumed to have a significant influence on the growth of impurity phases, to simplify the discussion on the first application of Bayesian optimization to the synthesis process of superconducting materials. Bayesian optimization was performed using the graphical user interface-based application, BOXVIA [12]. BOXVIA enables the use of Bayesian optimization and the visualization of optimization results without any source code preparation or computing environment construction. Furthermore, through visualization of the optimization process for the phase purity maximization of P-doped Ba122 polycrystalline bulks, we discuss the advantages of applying Bayesian optimization to the synthesis process of superconducting materials.

2. Materials and methods

2.1. Sample preparation and evaluation methods

Polycrystalline bulk $BaFe_2(As,P)_2$ samples were prepared by sintering the mechanically alloyed precursor powders. In an Ar-atmosphere glove box, an elemental metal mixture of Ba, Fe, As, and P with a molar ratio of Ba:Fe:As:P = 1:2:1.34:0.66 (i.e., a nominal composition of $BaFe_2(As_{0.67}P_{0.33})_2$) was ball-milled with high energy using a planetary ball-mill apparatus [42,43]. The precursor powder was formed into a disk-shaped pellet with a diameter and thickness of 7 mm and 1 mm, respectively. The pellet was vacuum-sealed in a quartz tube. Each sample was heated for 2 h to the designated heating temperature suggested by BOXVIA and then held for 48 h before furnace cooling. The constituent phases of the samples were evaluated by powder X-ray diffraction (XRD; D2 PHASER, Bruker) using Cu-K_α radiation with a λ of 1.5418 Å. The lattice constants and phase purity were quantitatively evaluated using Rietveld analysis (DIFFRAC.TOPAS). The chemical composition was evaluated by energy-dispersive X-ray spectroscopy (EDX) on the polished cross-sections of the samples.

2.2. Bayesian optimization

The experimental result y_i (i denotes the number of experiments) is defined as $y_i = f(\boldsymbol{x}_i)$, where $\boldsymbol{x}_i$ is an arbitrary experimental condition, and f is a black-box function. In this study, y_i is the phase purity, and $\boldsymbol{x}_i$ is the temperature of the heat-treatment. Bayesian optimization considers f an objective function and maximizes/minimizes y_i using Gaussian process regression (GPR) [44]. GPR models a black-box function as a function represented by mean and covariance functions.

Here, we consider the case in which a dataset comprising $\boldsymbol{x}_i$ and y_i obtained from n experiments is available. The experimental conditions and results in the dataset are expressed using vectors $\boldsymbol{x}_{1:n} = (\boldsymbol{x}_1, \boldsymbol{x}_2, \ldots, \boldsymbol{x}_n)$ and $\boldsymbol{y}_{1:n} = (y_1, y_2, \ldots, y_n)$, respectively. Through GPR, the probability density function (PDF) of $\boldsymbol{y}_{1:n}$, which is called the prior distribution, is expressed as follows:

$$\boldsymbol{y}_{1:n} \sim N(\boldsymbol{0}, \boldsymbol{K}), \tag{1}$$

where $N(\boldsymbol{0}, \boldsymbol{K})$ represents the multivariate Gaussian distribution of the mean vector $\boldsymbol{0}$ and covariance matrix $\boldsymbol{K}$, which is defined as

$$\boldsymbol{K} = \begin{bmatrix} k(\boldsymbol{x}_1, \boldsymbol{x}_1) & \cdots & k(\boldsymbol{x}_1, \boldsymbol{x}_n) \\ \vdots & \ddots & \vdots \\ k(\boldsymbol{x}_n, \boldsymbol{x}_1) & \cdots & k(\boldsymbol{x}_n, \boldsymbol{x}_n) \end{bmatrix}. \tag{2}$$

where $k(\boldsymbol{x}_i, \boldsymbol{x}_j)$ is the kernel function representing the correlation

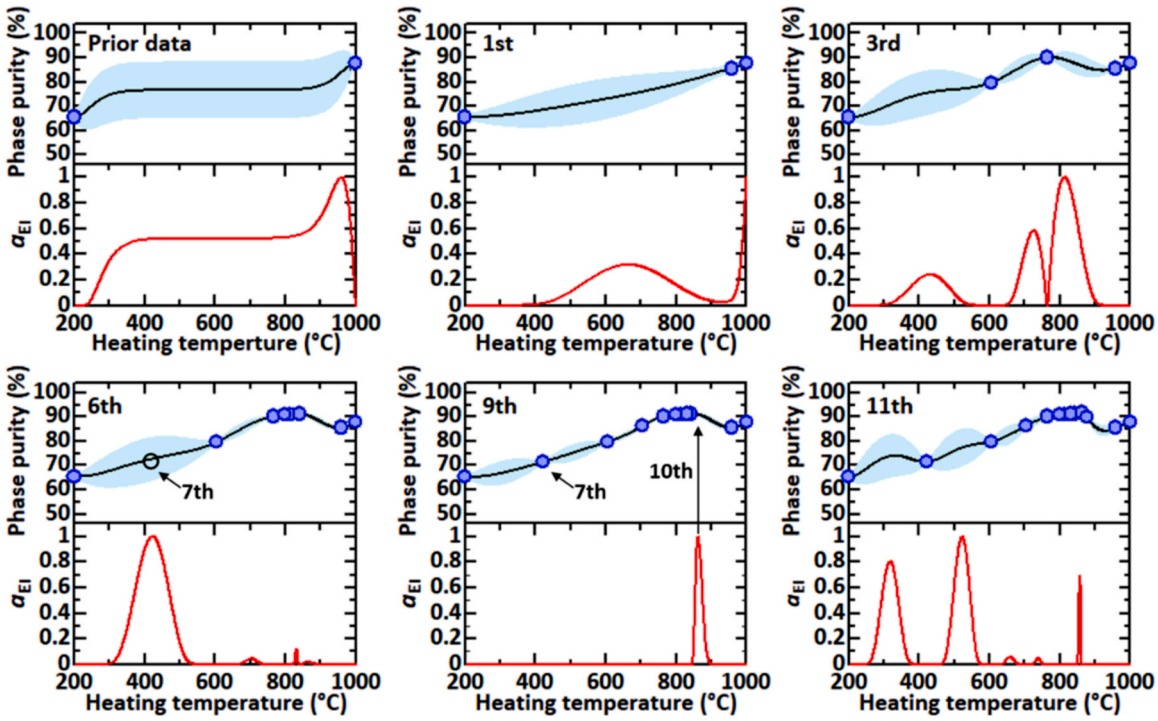

Fig. 6. Mean functions, standard deviations, and acquisition functions calculated by Gaussian process regression. The blue points represent the phase purity acquired up to the respective number of experiments. The black lines represent mean functions, and the light blue areas represent their standard deviations. The red lines show the acquisition functions normalized from 0 to 1.

between any two experimental conditions $\boldsymbol{x}_i$ and $\boldsymbol{x}_j$. This study used the following Matérn 5/2 kernel function, commonly used for Bayesian optimization [3,44,45].

$$k(\boldsymbol{x}_i,\boldsymbol{x}_j)=\alpha^2\left(1+\frac{\sqrt{5}\|\boldsymbol{x}_i-\boldsymbol{x}_j\|}{\beta}+\frac{5\|\boldsymbol{x}_i-\boldsymbol{x}_j\|^2}{3\beta^2}\right)\exp\left(-\frac{\sqrt{5}\|\boldsymbol{x}_i-\boldsymbol{x}_j\|}{\beta}\right), \quad (3)$$

where $||\bullet||$ denotes Euclidean distance, and α and β are hyperparameters dynamically determined during the optimization process [44].

When an arbitrary $\boldsymbol{x}_*$ is newly obtained, $\boldsymbol{y}_{1:n}$ and y_* can be joined by the properties of Gaussian processes [40] as

$$\begin{bmatrix}\boldsymbol{y}_{1:n}\\ y_*\end{bmatrix}\sim N\left(\boldsymbol{0},\begin{bmatrix}\boldsymbol{K} & \boldsymbol{k}\\ \boldsymbol{k}^{\mathrm{T}} & k(\boldsymbol{x}_*,\boldsymbol{x}_*)\end{bmatrix}\right), \quad (4)$$

where $\boldsymbol{k}$ is a vector defined as

$$\boldsymbol{k}=[k(\boldsymbol{x}_*,\boldsymbol{x}_n)\quad k(\boldsymbol{x}_*,\boldsymbol{x}_n)\quad\cdots\quad k(\boldsymbol{x}_*,\boldsymbol{x}_n)]^T, \quad (5)$$

According to Eqs. (4) and (5), the conditional PDF of y_* under the given data of $\boldsymbol{x}_*$, $\boldsymbol{x}_{1:n}$, and $\boldsymbol{y}_{1:n}$ (known as the posterior distribution) is calculated as follows:

$$p(y_*|\boldsymbol{x}_*,\boldsymbol{x}_{1:n},\boldsymbol{y}_{1:n})=N\left(\mu_n(\boldsymbol{x}_*),\sigma_n^2(\boldsymbol{x}_*)\right), \quad (6)$$

where $\mu_n(\boldsymbol{x}_*)$ and $\sigma_n^2(\boldsymbol{x}_*)$ denote the posterior mean and the variance, respectively. The mean is calculated as

$$\mu_n(\boldsymbol{x}_*)=\boldsymbol{k}^{\mathrm{T}}\boldsymbol{K}^{-1}\boldsymbol{y}_{1:n}, \quad (7)$$

and the variance is calculated as

$$\sigma_n^2(\boldsymbol{x}_*)=k(\boldsymbol{x}_*,\boldsymbol{x}_*)-\boldsymbol{k}^{\mathrm{T}}\boldsymbol{K}^{-1}\boldsymbol{k} \quad (8)$$

In simple terms, $\mu_n(\boldsymbol{x}_*)$ and $\sigma_n^2(\boldsymbol{x}_*)$ (or $\sigma_n(\boldsymbol{x}^*)$) are the mean and variance (or standard deviation) of a Gaussian distribution representing the predicted result of an experiment conducted under condition $\boldsymbol{x}_*$.

Bayesian optimization uses an acquisition function to determine the next experimental condition $\boldsymbol{x}(n+1)$. Although several types of acquisition functions have been proposed [44], this study uses the expected improvement (EI) acquisition function because the EI function is widely used in various applications [2,7,8,45]. The EI acquisition function for maximizing y_i is expressed as [44,46]:

$$a_{\mathrm{EI}}(\boldsymbol{x}_*)=\begin{cases}(\mu_n(\boldsymbol{x}_*)-f(\boldsymbol{x}^{\max})-\xi)\Phi(Z)+\sigma_n(\boldsymbol{x}_*)\phi(Z) & (\sigma_n(\boldsymbol{x}_*)>0)\\ 0 & (\sigma_n(\boldsymbol{x}_*)=0)\end{cases}, \quad (9)$$

$$Z=\begin{cases}\dfrac{\mu_n(\boldsymbol{x}_*)-f(\boldsymbol{x}^{\max})-\xi}{\sigma_n(\boldsymbol{x}_*)} & (\sigma_n(\boldsymbol{x}_*)>0)\\ 0 & (\sigma_n(\boldsymbol{x}_*)=0)\end{cases}, \quad (10)$$

where $\phi(\bullet)$ and $\Phi(\bullet)$ represent the PDF and the cumulative distribution functions, respectively. $\boldsymbol{x}^{\max}$ is the experimental condition that provides the maximum y_i in the dataset obtained in n experiments. The EI acquisition function considers both the probability that $f(\boldsymbol{x}_*)$ improves from $f(\boldsymbol{x}^{\max})$ and the amount of improvement. The next experimental condition of $\boldsymbol{x}_{n+1}$ is defined as $\boldsymbol{x}_*$, which maximizes $a_{\mathrm{EI}}(\boldsymbol{x}_*)$. In typical human-based optimization, to improve y_i, the next experiment is conducted under conditions close to $\boldsymbol{x}^{\max}$ (local optimization) or conditions with fewer data (global search). In Bayesian optimization, local optimization and global searches are well balanced by the acquisition function using $\mu_n(\boldsymbol{x}_*)$ and $\sigma_n(\boldsymbol{x}_*)$. Local optimization is encouraged when $\mu_n(\boldsymbol{x}_*)$ is large, whereas global search is encouraged when $\sigma_n(\boldsymbol{x}_*)$ is large. In addition, the EI acquisition function can control the tradeoff between local optimization and global search by tuning a hyperparameter. ξ (≥ 0).

In this study, calculations for the Bayesian optimization described above to maximize the phase purity of P-doped Ba122 were performed using BOXVIA [10]. ξ was set to 0.01, which is the default value for BOXVIA. The range of possible temperatures for the heat treatment was set at 200–1000 °C, which is sufficiently wide to avoid human bias. The increment in the temperature condition was set to 1 °C (i.e., 800

candidates were available). When the same conditions were suggested by the Bayesian optimization as those for which the data had already been obtained, the existing data were used again because the reproducibility of the experimental results was assumed to be high.

2.3. Flowchart

Fig. 1 shows the procedure for obtaining high-phase-purity P-doped Ba122 polycrystalline bulk materials using Bayesian optimization. Preliminary experiments were conducted to prepare a dataset with $\boldsymbol{x}_{1:n}$ and $\boldsymbol{y}_{1:n}$ to calculate the initial prior distribution. We set $\boldsymbol{x}_{1:n}$ of the prior data to $\boldsymbol{x}_{1:2} = (200, 1000)$. The prior dataset was used for Bayesian optimization to obtain the first temperature condition for heat-treatment. The phase purity of the heat-treated samples was measured using Rietveld analysis. The temperature conditions and measured phase purity were then added to the dataset. The phase purity was maximized by iterating the cycle of Bayesian optimization, conducting heat-treatment at the suggested temperature, and analyzing the samples.

3. Results and discussions

3.1. Evaluations of the samples

Fig. 2 shows the heating temperature dependence of the (a) phase purity, (b) *a*-axis length, and (c) *c*-axis length of the samples after 12 iterations. The mean function and standard deviation shown in Fig. 2(a) are obtained by GPR. The phase purities of the samples heated at 200 °C and 1000 °C, which were prepared as prior data, were 65.4 % and 87.7 %, respectively. The iteration cycle using Bayesian optimization revealed that the phase purity increased with the heat-treatment temperature below ~900 °C. High phase purity can be obtained at 750–870 °C. A maximum phase purity of 91.3 % was obtained at 863 °C after 10 iterations. Low phase purity was observed above ~900 °C, suggesting that the formation of impurity phases such as Fe_2P was enhanced at high temperatures. Both the *a*- and *c*-axis lengths tended to become shorter and closer to the lattice constants of single crystals for samples with high phase purity. The *a*- and *c*-axis lengths of P-doped Ba122 decrease with increasing P doping [47]. Fig. 3 shows the powder XRD patterns of the samples. The Ba122 phase was the main phase in all the samples. In contrast, the Fe_2P phase was found to be an impurity phase, particularly in samples with lesser phase impurities. These results suggest that a decrease in the impurity Fe_2P phase improves the phase purity of Ba122 and the P doping level in the Ba122 phase.

Fig. 4 shows the electron reflection images obtained by scanning electron microscopy and the elemental mapping images of the corresponding regions by EDX analysis for the sample with the highest phase purity (heat treatment temperature: 863 °C). In the Fe and P elemental mapping, no distribution of Ba and As was observed in the region of approximately 1–5 μm, where Fe and P are typically enriched, corresponding to the Fe_2P phase.

To demonstrate the superconducting property in $BaFe_2(As,P)_2$ bulks with improved phase purity, resistivity measurement of dense bulk sample synthesized at 863 °C under 50 MPa was performed by dipping in liquid helium. Fig. 5 shows the temperature dependence of resistivity for the $BaFe_2(As,P)_2$ bulk sample sintered at 863 °C. The bulk sample exhibited superconducting transition at high temperature of 30.6 K, which is among the highest in polycrystalline samples and comparable to T_c (31 K) of optimally doped single crystals ($x = 0.33$ in $BaFe_2(As_{1-x}P_x)_2$) [47]. This result indicates that, owing to the high purity of the bulk sample, phosphorous was successfully doped in the lattice and its doping level is close to the nominal composition. The zero resistance temperature (27.5 K) is as high as those of thin films (21.2–26.5 K) with phosphorous doping level $x = 0.28$–0.45 [30,34], however lower than that of the single crystal (~30 K [47]). Residual-resistance ratio (*RRR*) of the bulk sample is 4.25, which is lower than the in-plane *RRR* of the single crystal (~5.4 [47]). Since the bulk sample is randomly oriented polycrystal, electromagnetic anisotropy and grain-boundaries are considered to affect the broadened resistive transition and lower *RRR* compared to those of single crystals.

3.2. Discussions of the optimization process using Bayesian optimization

Fig. 6 shows the variations in the mean function, standard deviation, and acquisition function calculated during the optimization process of the phase purity of the P-doped Ba122 polycrystalline bulks for the number of experiments. The acquisition function was normalized from 0 to 1. The experimental results were frequently within the standard deviation calculated in a previous experiment. For example, Fig. 6 shows the results of the 7th experiment as a hollow circle on a graph drawn after the 6th experiment. This result indicates that the temperature dependence of phase purity can be roughly predicted by referring to the mean function and its standard deviation without conducting several experiments covering the possible temperature range. Furthermore, the mean function and its standard deviation calculated after the 11th experiment suggest a significant increase in phase purity cannot be expected in further experiments. Therefore, further improvement of the phase purity of P-doped Ba122 requires simultaneous optimization of other experimental conditions, such as the parameters for mechanical alloying, the treatment time, and the heating rate.

As described in Section 3.1, a maximum phase purity of 91.3 % was obtained at 863 °C. Bayesian optimization enabled the identification of the temperature conditions in 1-°C increments from a wide search range of 800 °C in a total of 13 experiments (2 preliminary and 11 iterative). This efficient and fine optimization of the phase purity was achieved by balancing the local optimization and global search by the acquisition function, as shown in Fig. 6. The 7th and 10th experimental conditions were suggested by global search and local optimization, respectively. The properties of superconducting materials could be significantly affected by slight differences in their synthesis processes. Nakane et al. [48] reported that the J_c of a superconducting tape could be more than doubled with only a change of 5 °C in the heat-treatment temperature. Ishida et al. [28] demonstrated that a slight change in the doping level of Ba122 leads to improved superconducting properties. However, investigations under a wide range of experimental conditions are also important to determine the optimum conditions for improving superconducting properties due to the possibility of multiple peaks in the properties, as reported by Iimura et al. [49]. Therefore, Bayesian optimization, which can obtain finely optimal conditions through local optimization and global search with a small number of experiments, is useful for optimizing superconducting materials.

Generally, the advantage of Bayesian optimization is that the number of experiments can be significantly reduced compared with conventional methods. For example, Refs. [31,32] reported that Bayesian optimization reduced the number of experiments by factors of approximately 100 and 60, respectively. In the typical conventional strategy for the synthesis process optimization of superconducting materials, to avoid an increase in the number of experiments, optimal conditions are searched within a narrow range where the best result is expected based on human experience and/or preliminary experiments. In the case of improving the phase purity of P-doped Ba122, the search range of heat-treatment temperature was narrowly set at 600–1000 °C, for example, based on the knowledge that the phase purity is not expected to improve at low temperatures. When only the heat treatment temperature is designed, the optimal conditions are potentially found by the conventional strategy, which narrows the search range based on experience with a similar number of experiments as those of the Bayesian optimization. However, when the number of design parameters for improving phase purity increases, the narrow search ranges (i.e., human bias) prevent researchers from discovering unexpected optimal conditions. In addition, some design parameters, such as the heating rate, make it difficult to narrow the search ranges based on human experience because their effects on the superconducting properties are unclear,

which may lead to a range that does not contain the optimal values. This problem also arises in the fabrication of other forms of superconducting materials (e.g., the gas flow rate in the fabrication of thin films) and in new process applications. Bayesian optimization can provide optimal conditions with a small number of experiments and without narrow constraints, even when the number of design parameters increases. Therefore, from the above discussion, Bayesian optimization is promising as a powerful tool for maximizing the phase purity of P-doped Ba122 and for the process optimization of any superconducting material.

4. Conclusions

This study improves the phase purity of the P-doped Ba122 polycrystalline bulk as a model case for the application of Bayesian optimization to the synthesis process of superconducting materials. The phase purity improved to 91.3 %, and the optimal temperature was identified to be 863 °C by only 13 experiments. The XRD and EDX measurements demonstrated that the impurity phase was dominated by Fe_2P. Through the reduction of the impurity phase, including phosphorus, samples with a high phase purity resulted in a doping level closer to the nominal composition of the Ba122 phase. Bayesian optimization provided a global variation in the phase purity depending on the heat-treatment temperature and a fine local optimum temperature in 1-°C increments with fewer experiments. The results demonstrate the effectiveness of Bayesian optimization for the synthesis process of superconducting materials, which requires the global search and local optimization of the experimental conditions. Therefore, Bayesian optimization is expected to contribute to efficiently enhancing the superconducting properties when applied to synthesis processes with several design parameters in future work.

CRediT authorship contribution statement

Akimitsu Ishii: Methodology, Software, Formal analysis, Data Curation, Writing - Original Draft, Visualization. **Shinjiro Kikuchi**: Conceptualization, Methodology, Validation, Investigation, Data Curation, Writing - Original Draft, Visualization. **Akinori Yamanaka**: Conceptualization, Writing - Review & Editing, Supervision. **Akiyasu Yamamoto**: Conceptualization, Investigation, Resources, Writing - Review & Editing, Supervision, Project administration, Funding acquisition.

Declaration of Competing Interest

The authors declare that they have no known competing financial interests or personal relationships that could have appeared to influence the work reported in this paper.

Acknowledgement

This work was supported by Strategic Basic Research Programs, Core Research for Evolutional Science and Technology (CREST) (funding agency: JST, Japan) [grant number: JPMJCR18J4].

References

[1] G. Lambard, T.T. Sasaki, K. Sodeyama, T. Ohkubo, K. Hono, Optimization of direct extrusion process for Nd-Fe-B magnets using active learning assisted by machine learning and Bayesian optimization, Scr. Mater. 209 (2022), 114341, https://doi.org/10.1016/j.scriptamat.2021.114341.

[2] K. Osada, K. Kutsukake, J. Yamamoto, S. Yamashita, T. Kodera, Y. Nagai, T. Horikawa, K. Matsui, I. Takeuchi, T. Ujihara, Adaptive Bayesian optimization for epitaxial growth of Si thin films under various constraints, Mater. Today Commun. 25 (2020), 101538, https://doi.org/10.1016/j.mtcomm.2020.101538.

[3] J. Chang, P. Nikolaev, J. Carpena-Núñez, R. Rao, K. Decker, A.E. Islam, J. Kim, M. A. Pitt, J.I. Myung, B. Maruyama, Efficient closed-loop maximization of carbon nanotube growth rate using Bayesian optimization, Sci. Rep. 10 (2020) 9040, https://doi.org/10.1038/s41598-020-64397-3.

[4] K. Wang, A.W. Dowling, Bayesian optimization for chemical products and functional materials, Curr. Opin. Chem. Eng. 36 (2022), 100728, https://doi.org/10.1016/j.coche.2021.100728.

[5] Y. Xie, C. Zhang, H. Deng, B. Zheng, J.W. Su, K. Shutt, J. Lin, Accelerate synthesis of metal–organic frameworks by a robotic platform and Bayesian optimization, ACS Appl. Mater. Interfaces 13 (2021) 53485–53491, https://doi.org/10.1021/acsami.1c16506.

[6] J.R. Deneault, J. Chang, J. Myung, D. Hooper, A. Armstrong, M. Pitt, B. Maruyama, Toward autonomous additive manufacturing: Bayesian optimization on a 3D printer, MRS Bull. 46 (2021) 566–575, https://doi.org/10.1557/s43577-021-00051-1.

[7] A.E. Gongora, B. Xu, W. Perry, C. Okoye, P. Riley, K.G. Reyes, E.F. Morgan, K. A. Brown, A Bayesian experimental autonomous researcher for mechanical design, Sci. Adv. 6 (2020) eaaz1708, https://doi.org/10.1126/sciadv.aaz1708.

[8] S. Subianto, C. Li, D.R.C. Leal, S. Rana, S. Gupta, R. He, S. Venkatesh, A. Sutti, Optimizing a high-entropy system: software-assisted development of highly hydrophobic surfaces using an amphiphilic polymer, ACS Omega 4 (2019) 15912–15922, https://doi.org/10.1021/acsomega.9b01978.

[9] B. Shahriari, K. Swersky, Z. Wang, R.P. Adams, N. de Freitas, Taking the human out of the loop: a review of Bayesian optimization, Proc. IEEE 104 (2016) 148–175, https://doi.org/10.1109/JPROC.2015.2494218.

[10] A. Ishii, R. Kamijyo, A. Yamanaka, A. Yamamoto, BOXVIA: Bayesian optimization executable and visualizable application, SoftwareX 18 (2022), 101019, https://doi.org/10.1016/j.softx.2022.101019.

[11] K. Terayama, K. Tsuda, R. Tamura, Efficient recommendation tool of materials by an executable file based on machine learning, Jpn. J. Appl. Phys. 58 (2019), 098001, https://doi.org/10.7567/1347-4065/ab349b.

[12] D. Matera, M. Bonura, R. Černý, S.M. Walker, F. Buta, D. LeBoeuf, X. Chaud, E. Giannini, C. Senatore, High-field superconductivity in C-doped MgB2 bulk samples prepared by a rapid synthesis route, Sci. Rep. 10 (2020) 17656, https://doi.org/10.1038/s41598-020-74300-9.

[13] M. Rotter, M. Pangerl, M. Tegel, D. Johrendt, Superconductivity and crystal structures of $(Ba_{1-x}K_x)Fe_2As_2$ ($x = 0$–1), Angew. Chem. Int. Ed. 47 (2008) 7949–7952, https://doi.org/10.1002/anie.200803641.

[14] M. Rotter, M. Tegel, D. Johrendt, Superconductivity at 38 K in the iron arsenide $(Ba_{1-x}K_x)Fe_2As_2$, Phys. Rev. Lett. 101 (2008), 107006, https://doi.org/10.1103/PhysRevLett.101.107006.

[15] Y. Kamihara, T. Watanabe, M. Hirano, H. Hosono, Iron-based layered superconductor $La[O_{1-x}F_x]FeAs$ ($x = 0.05$–0.12) with $T_c = 26$ K, J. Am. Chem. Soc. 130 (2008) 3296–3297, https://doi.org/10.1021/ja800073m.

[16] H. Hosono, A. Yamamoto, H. Hiramatsu, Y. Ma, Recent advances in iron-based superconductors toward applications, Mater. Today 21 (2018) 278–302, https://doi.org/10.1016/j.mattod.2017.09.006.

[17] M. Nakajima, S. Ishida, T. Tanaka, K. Kihou, Y. Tomioka, T. Saito, C.H. Lee, H. Fukazawa, Y. Kohori, T. Kakeshita, A. Iyo, T. Ito, H. Eisaki, S. Uchida, Normal-state charge dynamics in doped $BaFe_2As_2$: roles of doping and necessary ingredient for superconductivity, Sci. Rep. 4 (2014) 5873, https://doi.org/10.1038/srep05873.

[18] A.S. Sefat, R. Jin, M.A. McGuire, B.C. Sales, D.J. Singh, D. Mandrus, Superconductivity at 22 K in Co-doped $BaFe_2As^2$ crystals, Phys. Rev. Lett. 101 (2008), 117004, https://doi.org/10.1103/PhysRevLett.101.117004.

[19] S. Jiang, H. Xing, G. Xuan, C. Wang, Z. Ren, C. Feng, J. Dai, Z. Xu, G. Cao, Superconductivity up to 30 K in the vicinity of the quantum critical point in $BaFe_2(As_{1-x}P_x)_2$, J. Phys. Condens. Matter 21 (2009), 382203, https://doi.org/10.1088/0953-8984/21/38/382203.

[20] H.Q. Yuan, J. Singleton, F.F. Balakirev, S.A. Baily, G.F. Chen, J.L. Luo, N.L. Wang, Nearly isotropic superconductivity in $(Ba,K)Fe_2As_2$, Nature 457 (2009) 565–568, https://doi.org/10.1038/nature07676.

[21] K. Vinod, A.T. Satya, S. Sharma, C.S. Sundar, A. Bharathi, Upper critical field anisotropy in $BaFe_{2-x}Co_xAs_2$ single crystals synthesized without flux, Phys. Rev. B 84 (2011), 012502, https://doi.org/10.1103/PhysRevB.84.012502.

[22] C. Tarantini, A. Gurevich, J. Jaroszynski, F. Balakirev, E. Bellingeri, I. Pallecchi, C. Ferdeghini, B. Shen, H.H. Wen, D.C. Larbalestier, Significant enhancement of upper critical fields by doping and strain in iron-based superconductors, Phys. Rev. B 84 (2011), 184522, https://doi.org/10.1103/PhysRevB.84.184522.

[23] M.M. Altarawneh, K. Collar, C.H. Mielke, N. Ni, S.L. Bud'Ko, P.C. Canfield, Determination of anisotropic H_{c2} up to 60T in $Ba_{0.55}K_{0.45}Fe_2As_2$ single crystals, Phys. Rev. B 78 (2008), 220505, https://doi.org/10.1103/PhysRevB.78.220505.

[24] L. Fang, Y. Jia, C. Chaparro, G. Sheet, H. Claus, M.A. Kirk, A.E. Koshelev, U. Welp, G.W. Crabtree, W.K. Kwok, S. Zhu, H.F. Hu, J.M. Zuo, H.-H. Wen, B. Shen, High, magnetic field independent critical currents in $(Ba,K)Fe_2As_2$ crystals, Appl. Phys. Lett. 101 (2012), 012601, https://doi.org/10.1063/1.4731204.

[25] A. Yamamoto, J. Jaroszynski, C. Tarantini, L. Balicas, J. Jiang, A. Gurevich, D. C. Larbalestier, R. Jin, A.S. Sefat, M.A. McGuire, B.C. Sales, D.K. Christen, D. Mandrus, Small anisotropy, weak thermal fluctuations, and high field superconductivity in Co-doped iron pnictide $Ba(Fe_{1-x}Co_x)_2As_2$, Appl. Phys. Lett. 94 (2009), 062511, https://doi.org/10.1063/1.3081455.

[26] T. Katase, Y. Ishimaru, A. Tsukamoto, H. Hiramatsu, T. Kamiya, K. Tanabe, H. Hosono, Advantageous grain boundaries in iron pnictide superconductors, Nat. Commun. 2 (2011) 409, https://doi.org/10.1038/ncomms1419.

[27] S. Lee, J. Jiang, J.D. Weiss, C.M. Folkman, C.W. Bark, C. Tarantini, A. Xu, D. Abraimov, A. Polyanskii, C.T. Nelson, Y. Zhang, S.H. Baek, H.W. Jang, A. Yamamoto, F. Kametani, X.Q. Pan, E.E. Hellstrom, A. Gurevich, C.B. Eom, D. C. Larbalestier, Weak-link behavior of grain boundaries in superconducting Ba

$(Fe_{1-x}Co_x)_2As_2$ bicrystals, Appl. Phys. Lett. 95 (2009), 212505, https://doi.org/10.1063/1.3262953.
[28] S. Ishida, D. Song, H. Ogino, A. Iyo, H. Eisaki, M. Nakajima, J. Shimoyama, M. Eisterer, Doping-dependent critical current properties in K, Co, and P-doped $BaFe_2As_2$ single crystals, Phys. Rev. B 95 (2017), 014517, https://doi.org/10.1103/PhysRevB.95.014517.
[29] M. Kano, Y. Kohama, D. Graf, F. Balakirev, A.S. Sefat, M.A. McGuire, B.C. Sales, D. Mandrus, S.W. Tozer, Anisotropy of the upper critical field in a Co-doped $BaFe_2As_2$ single crystal, J. Phys. Soc. Jpn. 78 (2009), 084719, https://doi.org/10.1143/JPSJ.78.084719.
[30] M. Miura, S. Adachi, T. Shimode, K. Wada, A. Takemori, N. Chikumoto, K. Nakao, K. Tanabe, Anisotropy and superconducting properties of $BaFe_2(As_{1-x}P_x)_2$ films with various phosphorus contents, Appl. Phys. Express 6 (2013), 093101, https://doi.org/10.7567/APEX.6.093101.
[31] A. Sakagami, T. Kawaguchi, M. Tabuchi, T. Ujihara, Y. Takeda, H. Ikuta, Critical current density and grain boundary property of $BaFe_2(As,P)_2$ thin films, Phys. C 494 (2013) 181–184, https://doi.org/10.1016/j.physc.2013.04.047.
[32] H. Sato, H. Hiramatsu, T. Kamiya, H. Hosono, High critical-current density with less anisotropy in $BaFe_2(As,P)_2$ epitaxial thin films: Effect of intentionally grown c-axis vortex-pinning centers, Appl. Phys. Lett. 104 (2014), 182603, https://doi.org/10.1063/1.4875956.
[33] S. Adachi, T. Shimode, Y. Murai, N. Chikumoto, K. Tanabe, Chemical reaction between $BaFe_2(As,P)_2$ superconducting thin film and LSAT substrate, Phys. C 502 (2014) 31–35, https://doi.org/10.1016/j.physc.2014.04.028.
[34] H. Sato, H. Hiramatsu, T. Kamiya, H. Hosono, Enhanced critical-current in P-doped $BaFe_2As_2$ thin films on metal substrates arising from poorly aligned boundaries, Sci. Rep. 6 (2016) 36828, https://doi.org/10.1038/srep36828.
[35] K. Iida, H. Sato, C. Tarantini, J. Hänisch, J. Jaroszynski, H. Hiramatsu, B. Holzapfel, H. Hosono, High-field transport properties of a P-doped $BaFe_2As_2$ films on technical substrate, Sci. Rep. 7 (2017) 39951, https://doi.org/10.1038/srep39951.
[36] M. Miura, G. Tsuchiya, T. Harada, K. Tanabe, M. Kiuchi, T. Matsushita, Enhanced critical current density in $BaFe_2(As_{0.66}P_{0.33})_2$ nanocomposite superconducting films, Supercond. Sci. Technol. 32 (2019), 064005, https://doi.org/10.1088/1361-6668/ab0faf.
[37] W. Zhang, Y. Wei, T. Xie, Z. Liu, D. Gong, X. Ma, D. Hu, P. Čermák, A. Schneidewind, G. Tucker, S. Meng, Z. Huesges, Z. Lu, J. Song, W. Luo, L. Xu, Z. Zhu, X. Yin, H.F. Li, Y.F. Yang, H. Luo, S. Li, Unconventional antiferromagnetic quantum critical point in $Ba(Fe_{0.97}Cr_{0.03})_2(As_{1-x}P_x)_2$, Phys. Rev. Lett. 122 (2019), 037001, https://doi.org/10.1103/PhysRevLett.122.037001.
[38] V. Grinenko, K. Iida, F. Kurth, D.V. Efremov, S.L. Drechsler, I. Cherniavskii, I. Morozov, J. Hänisch, T. Förster, C. Tarantini, J. Jaroszynski, B. Maiorov, M. Jaime, A. Yamamoto, I. Nakamura, R. Fujimoto, T. Hatano, H. Ikuta, R. Hühne, Selective mass enhancement close to the quantum critical point in $BaFe_2(As_{1-x}P_x)_2$, Sci. Rep. 7 (2017) 4589, https://doi.org/10.1038/s41598-017-04724-3.
[39] S. Kasahara, H.J. Shi, K. Hashimoto, S. Tonegawa, Y. Mizukami, T. Shibauchi, K. Sugimoto, T. Fukuda, T. Terashima, A.H. Nevidomskyy, Y. Matsuda, Electronic nematicity above the structural and superconducting transition in $BaFe_2(As_{1-x}P_x)_2$, Nature 486 (2012) 382–385, https://doi.org/10.1038/nature11178.
[40] D. Contarino, C. Löhnert, D. Johrendt, A. Genovese, C. Bernini, A. Malagoli, M. Putti, Development and characterization of P-doped Ba-122 superconducting tapes, IEEE Trans. Appl. Supercond. 27 (2017) 1–4, https://doi.org/10.1109/TASC.2016.2633386.
[41] J.M. Allred, K.M. Taddei, D.E. Bugaris, S. Avci, D.Y. Chung, H. Claus, C. dela Cruz, M.G. Kanatzidis, S. Rosenkranz, R. Osborn, O. Chmaissem, Coincident structural and magnetic order in $BaFe_2(As_{1-x}P_x)_2$ revealed by high-resolution neutron diffraction, Phys. Rev. B 90 (2014), 104512, https://doi.org/10.1103/PhysRevB.90.104513.
[42] S. Tokuta, A. Yamamoto, Enhanced upper critical field in Co-doped Ba122 superconductors by lattice defect tuning, APL Mater. 7 (2019), 111107, https://doi.org/10.1063/1.5098057.
[43] S. Tokuta, Y. Shimada, A. Yamamoto, Evolution of intergranular microstructure and critical current properties of polycrystalline Co-doped $BaFe_2As_2$ through high-energy milling, Supercond. Sci. Technol. 33 (2020), 094010, https://doi.org/10.1088/1361-6668/aba545.
[44] C.E. Rasmussen, C.K.I. Williams, Gaussian processes for. Mach. Learn, MIT Press, 2006.
[45] A. Ishii, A. Yamanaka, E. Miyoshi, A. Yamamoto, Efficient estimation of material parameters using DMC-BO: application to phase-field simulation of solid-state sintering, Mater. Today Commun. 30 (2022), 103089, https://doi.org/10.1016/j.mtcomm.2021.103089.
[46] D.R. Jones, M. Schonlau, W.J. Welch, Efficient global optimization of expensive black-box functions, J. Glob. Optim. 13 (1998) 455–492, https://doi.org/10.1023/A:1008306431147.
[47] S. Kasahara, T. Shibauchi, K. Hashimoto, K. Ikada, S. Tonegawa, R. Okazaki, H. Shishido, H. Ikeda, H. Takeya, K. Hirata, T. Terashima, Y. Matsuda, Evolution from non-Fermi- to Fermi-liquid transport via isolvalent doping in $BaFe_2(As_{1-x}P_x)_2$ superconductors, Phys. Rev. B 81 (2010), 184519, https://doi.org/10.1103/PhysRevB.81.184519.
[48] T. Nakane, A. Matsumoto, H. Kitaguchi, H. Kumakura, Performance tuning and improvement of J_c-B characteristics for Bi-2212/Ag tapes by controlling the excess oxygen content, Supercond. Sci. Technol. 17 (2004) 29–34, https://doi.org/10.1088/0953-2048/17/1/005.
[49] S. Iimura, S. Matsuishi, H. Sato, T. Hanna, Y. Muraba, S.W. Kim, J.E. Kim, M. Takata, H. Hosono, Two-dome structure in electron-doped iron arsenide superconductors, Nat. Commun. 3 (2012) 943, https://doi.org/10.1038/ncomms1913.